



Kinetics of oxidation of vanillic acid by colloidal MnO_2 : correlation of micellar catalysis to the micellar properties of surfactants and mixed surfactants

Mohammed Hassan^{1,4} · Adnan Dahadha² · Mohammad Al-Dhoun¹ · Yazan Batineh¹ · Tamara R. Mfarej³

Received: 2 July 2021 / Accepted: 18 July 2021 / Published online: 24 July 2021
© Akadémiai Kiadó, Budapest, Hungary 2021

Abstract

The kinetics of oxidation of vanillic acid by colloidal MnO_2 in an acidic medium was investigated and used as a probe to study the micellar catalysis and its correlation to micellar properties of surfactants. Three surfactants were employed; cationic cetyltrimethylammonium bromide (CTAB), anionic sodium dodecylsulfate (SDS), and non-ionic Tween-20 (TW-20), and some compositions of the two mixed systems CTAB-TW-20 and SDS-TW-20. The micellar properties were studied using the conductivity method. The reaction rate was enhanced in the presence of the three surfactants and the mixed systems. The catalytic profiles of the pure and mixed surfactant systems could be used to estimate the critical micelle concentrations of surfactant catalytic systems. Nevertheless, the kinetic measurements could not detect the variations in the micellar structures that occur at post-micellar compositions. Overall, the mixed systems studied showed a negative deviation of ideality with synergistic interaction. Therefore, Rubingh equations were used to calculate the micellar mole fraction and interaction parameters in the mixed surfactant systems.

Keywords Micellar catalysis · Mixed surfactant systems · Colloidal MnO_2 · Vanillic acid · Redox reactions

✉ Mohammed Hassan
msaleh@philadelphia.edu.jo

¹ Faculty of Pharmacy, Philadelphia University, Amman, Jordan

² Department of Genetics and Biotechnology, Faculty of Science, Philadelphia University, Amman, Jordan

³ Department of Basic Sciences and Mathematics, Faculty of Science, Philadelphia University, Amman, Jordan

⁴ Department of Chemistry, Faculty of Science, Ibb University, Ibb, Yemen

Introduction

Surfactants are amphiphilic molecules that tend to aggregate at a specific concentration called critical micelle concentration (CMC). They have found diverse applications in different fields such as oil recovery [1], cosmetics, drug delivery, fabrication of nanoparticles, etc. [2]. One of the important fields of surfactant applications is the catalysis of chemical reactions. Surfactants were found to enhance reaction rates via different mechanisms; bringing the reactants in close contact by solubilizing them in the micro-micellar structure, offering an environment with appropriate dielectric constant on the micellar surface, and provide a suitable medium for stabilizing transition states [3]. In addition, the surfactant-enhanced selectivity for specific products of some chemical reactions has been reported [4, 5].

Mixed surfactant systems, mixtures of two different surfactants, were one of the strategies that have been used to develop the desired properties of single surfactants. Mixed surfactants often show deviation of the ideal mixtures leading to synergetic properties [6]. This deviation may result in the enhancement of the desired property by synergetic interaction between the two surfactants. For example, many mixed surfactant systems showed critical micelle concentrations below those of either component [7]. The synergetic behavior made mixed surfactants advantageous over single surfactants and received wider potential applications [8]. Though the presence of mixed micelles in these systems was well evidenced, the occurrence of a specific critical micelle concentration before their formation is still doubtful. Cui et al. revealed that in mixed surfactant systems, the micelles of the lowest CMC components start to form, then the molecules of the other component (with higher CMC) start to fuse with them [9]. Moreover, some mixed systems showed two CMCs; the first is enriched with lower CMC component and the other enriched with higher CMC component [10].

Micellar catalysis responds to the synergetic interaction between the components of the mixed system. It has been found that the catalytic effect of mixed surfactant depends on several factors; CMC, the electrostatic properties of the micellar surface, and shape and volume of mixed micelles, in addition to the nature of reactants and products [11].

The sensitive response of reaction rates of chemical reactions to the variations in the composition of mixed surfactant systems may offer a valuable technique to track the properties of these systems. For example, the CMC was evaluated with good precision using the catalytic profiles of surfactants and mixed surfactants [12, 13].

Oxidation–reduction (redox) reactions have been used extensively to track the micellar catalysis of surfactants and mixed surfactants systems [14]. The focus on redox reactions in this field is due to their accessible rates by simple techniques and the availability of required chemicals. Among these reactions, those that contain colloidal manganese dioxide have been well used as probes for micellar catalysis with many organic and bioorganic substrates [15–17]. The interesting properties of colloidal MnO_2 are its powerful oxidation for a wide variety of substrates in the neutral medium [18], ease of preparation and the well-defined peak in the UV–Vis spectrum centered close to 390 nm [19].

Vanillic acid (VA), 4-Hydroxy-3-methoxybenzoic acid, is a derivative of dihydroxybenzoic acid and is found in many plant species such as the roots of *Angelica Sinensis* and humans as catechins metabolite after drinking a green tea infusion [20]. It is usually synthesized by the oxidation of vanillin, the well-known flavoring agent.

In continuation of our research interest on micellar catalysis, we undertook this work to investigate the micellar catalysis on the oxidation of vanillic acid (VA) by colloidal manganese dioxide. Three types of surfactants were employed; cationic cetyltrimethylammonium bromide (CTAB), anionic sodium dodecylsulfate (SDS), and non-ionic Tween-20 (TW-20). Some compositions of the two mixed systems CTAB-TW-20 and SDS-TW-20 were also tested as catalysts. The micellar properties of the three surfactants and mixed surfactant systems were explored using conductivity measurements. Besides, we tried to shed light on the possibility of using kinetic measurements as a tool to study the variation of the micellar properties with the composition of either single or mixed surfactant systems.

Experimental

Materials

Vanillic acid (98%, Alfa Aesar), potassium permanganate (99%, AZ Chem), sodium thiosulfate (99%, Sigma-Aldrich), sulfuric acid (95–97%, Sigma-Aldrich), sodium sulfate (99%, Merck), SDS (99%, AZ Chem), CTAB (98%, S. d. fine. Chem. India), TW-20 (Molecular biology grade, Sigma-Aldrich) were used without further purification. Stock solutions of 0.01 mol dm^{-3} VA, $0.08 \times 10^{-2} \text{ mol dm}^{-3}$ sulfuric acid, 0.01 mol dm^{-3} potassium permanganate, $1.88 \times 10^{-2} \text{ mol dm}^{-3}$ sodium thiosulfate, 0.20 mol dm^{-3} sodium sulfate, 0.05 mol dm^{-3} SDS, 0.01 mol dm^{-3} CTAB, and 0.01 mol dm^{-3} TW-20 were prepared by dissolving the requisite amounts of each substance in doubly distilled water. Colloidal manganese dioxide was prepared by adopting a method reported by Perez-Benito and Arias method [21]. The original method involves mixing 10 mL of sodium thiosulfate and 20 mL of potassium permanganate and complete the volume to 2L. Indeed, the resultant prepared colloidal MnO_2 was found to be stable for at least a week. However, the oxidizing activity of the solution was found to decrease with elongating storing period. Hence, we considered preparing a fresh amount of 250 mL of the solution using proportional amounts of potassium permanganate and sodium thiosulfate solutions and use it within 48 h. The absorbance of the resultant solution was constant throughout its using period, indicating that colloidal MnO_2 does not undergo redox reaction with air oxygen.

Kinetic measurements

The kinetic investigation was carried out by adopting the conditions of the pseudo-first order model, in which the concentration of VA was always kept in large excess over that of colloidal MnO_2 . The above-prepared stock solutions were used to drive

the reaction and investigate the effects of various factors in its rate. In a 50 mL beaker, 1 mL VA, 0.20 mL sulfuric acid, 1.00 mL sodium sulfate, and 8.80 mL water were placed. The beaker was kept in a digital thermostated water bath (PRECISION GP20, *ThermoScientific*, USA) at ± 0.1 of the required experimental temperature. The stock solution of colloidal MnO_2 was also kept in the same thermostat. After reaching thermal equilibrium, 2.00 mL of colloidal MnO_2 was pipetted out and poured into the beaker with gentle stirring. The mixture's absorbance was then immediately monitored at different time intervals at 390 nm (λ_{max} of colloidal MnO_2) using AE-S90-2D spectrometer (*A and E Lab*, UK) and quartz sample cells. The effects of the concentrations oxidant, substrate, sulfuric acid, sodium sulfate, and surfactants on the reaction rate were examined in subsequent experimental runs by addition of specific varying volumes of each reagent in the account of the volume of water to ensure the total volume of the reaction mixture always being kept at 13.00 mL. The concentrations of surfactants were varied in ranges that center around the CMCs, to explore catalytic effect in the presence of pre- and post-micellar amounts. Each experimental run was repeated three times, and the average k_{obs} value was considered for further calculations. The mean percentage error in the measurements of k_{obs} was less than 3% of the average.

Results and discussion

Product identification and reaction stoichiometry

The stoichiometry of the reaction was estimated by preparing several reaction mixtures, in which the concentration of VA was kept constant while the concentration of colloidal MnO_2 was in excess and varied over a wide range. These solutions were stoppered and kept in a dark place for about 48 hrs to ensure the reaction completion. Then, the excess amounts of colloidal MnO_2 were titrated against a standardized sodium thiosulfate solution in the presence of dilute concentrations of sulfuric acid. The calculations indicated that 2 mol of vanillic acid react with one mole of Colloidal MnO_2 . One of the prepared mixtures was also tested with 2,4-dinitrophenylhydrazine and give no precipitate, which indicates the absence of aldehydic or ketonic carbonyl groups. Besides, bubbles were observed during the reaction, which is evidence of evolving carbon dioxide gas that results from eliminating the carboxylic group of VA.

The spectra of the reaction mixture taken at different time intervals and those of VA and colloidal MnO_2 are seen in Fig. 1. VA showed three peaks centered at wavelengths 215, 260, and 290 nm. With the progress of the reaction, the intensities of the three peaks diminished with time. The position of the band at 215 nm slightly shifted with time toward a shorter wavelength, while the positions of the two did not vary. The lower wavelength peak converted to a knee for the reaction mixture close to completion. The other two peaks almost disappeared in the spectrum of one of the solutions used to measure stoichiometry.

Two isosbestic points are observed at the two wavelengths 325 and 370 nm, indicating the conversion of VA to a product that absorbs at the range 320–370 nm.

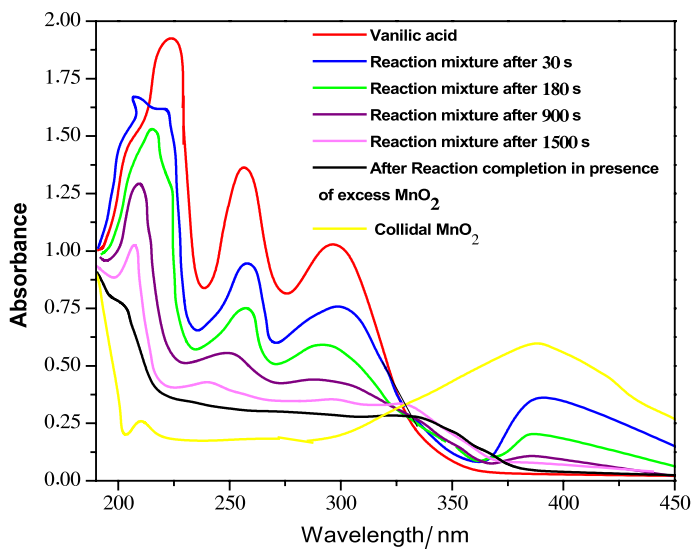
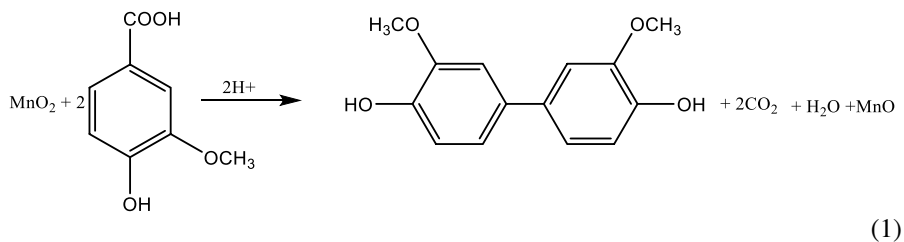


Fig. 1 UV–Visible spectra at 298 K of VA (7.70×10^{-4} mol dm^{-3}), colloidal MnO_2 (1.54×10^{-5} mol dm^{-3}), reaction mixture at different time intervals in 5.33×10^{-4} mol dm^{-3} H_2SO_4

Similar spectra were observed during the oxidation of VA with hydroxyl radicals [22]. The results were explained by the formation of a humic-like substance (HULIS), which possesses a higher number of conjugated double bonds, causing absorption at higher wavelengths. The possible mechanism of the formation of HULIS is the combination of two free radicals formed from an initial attack of colloidal MnO_2 on VA. Based on the above results, the equation that best describes the stoichiometry of the reaction can be written as follows:



Pseudo-first order curves

Overall, the pseudo-order model, in which the concentration of the substrate was always made \geq tenfold that of the oxidant, was followed. Fig. 2 shows the plots of absorbance against time at different concentrations of the oxidant and keeping other conditions fixed. The application of linear regression to the integrated first-order equation was successful to about 30% of reaction completion. The subsequent segments show curvature as the reaction progresses to completion. The deviation from linear regression in the oxidation reactions that involve colloidal MnO_2 was

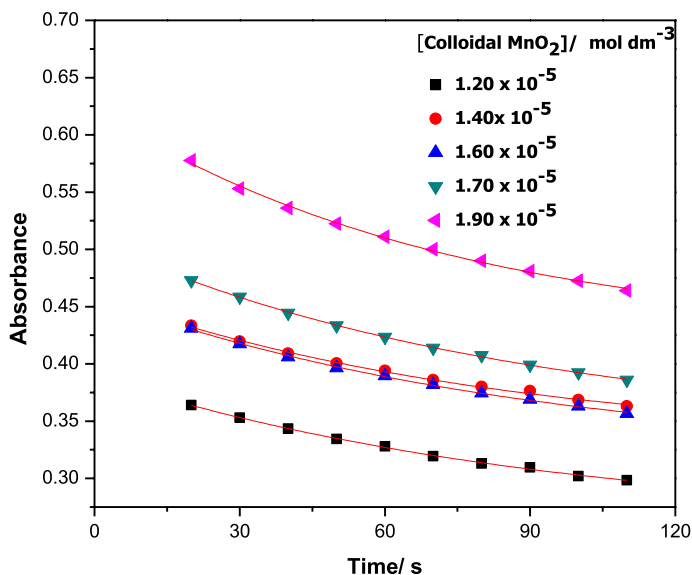


Fig. 2 Absorbance vs. time at different colloidal MnO_2 concentration; $[\text{VA}] = 7.70 \times 10^{-4} \text{ mol dm}^{-3}$, $[\text{H}_2\text{SO}_4] = 1.20 \times 10^{-5} \text{ mol dm}^{-3}$, $[\text{Na}_2\text{SO}_4] = 1.56 \times 10^{-2} \text{ mol dm}^{-3}$, at 298 K. The lines show the fitted experimental data to Eq. 2

previously observed [23]. This observation was explained by the slowing down of the reaction due to the adsorption of the product on the surface of colloidal particles of the oxidant. Therefore, the authors recommended using a modified equation that considers the desorption rate of the product from the surface of the oxidant. Besides, Charles L. Perrin [24] reported that the use of the usual first-order integrated equation is expected to deviate from linearity at later stages of reaction due to the continual error increase in estimating the value of $\ln A$. Therefore, they advised the use of non-linear regression to fit the absorbance-time curves to the following equation:

$$A = a + be^{-k_{\text{obs}}t} \quad (2)$$

Here A is the absorbance at time t , k_{obs} is the pseudo-order rate constant (observed rate constant), a and b are constants that depend on the reaction conditions. As shown in Fig. 1, the plots of A versus t were non-linearly fitted successfully to Eq. 2 with high regression coefficients ($r^2 \geq 0.99$). Consequently, this method was adopted to evaluate k_{obs} values from the kinetic experimental runs at different conditions.

Reaction order with respect to colloidal MnO_2

The concentration of colloidal MnO_2 was varied in the range 1.20×10^{-5} – $1.90 \times 10^{-5} \text{ mol dm}^{-3}$, with keeping other conditions fixed, to explore the effect of MnO_2 on the reaction rate. The obtained k_{obs} values were comparable within the standard deviation of the measurements, which indicates that the order with respect to the

oxidant is unity. The result that k_{obs} was independent of the concentration of the oxidant, indicates that the colloidal MnO_2 functions solely as an oxidizing agent and rules out the catalyzing effect on the reaction.

Reaction order with respect to VA

The plots between k_{obs} values and the molar concentration of VA in the absence and presence of surfactant are shown in Fig. 3. The plots could best be fitted successfully to straight lines at low concentrations of VA. However, they deviated from linearity and adopted a parabolic trend at higher VA concentrations. The plots were best fitted to the following equation:

$$k_{\text{obs}} = k[\text{VA}] + \bar{k}[\text{VA}]^2 \quad (3)$$

Here k and \bar{k} are constants related to the rate of the reaction. Equation 3 indicates that at low concentrations of VA, the second term becomes negligible, and the order of the reaction approaches unity. However, at relatively higher VA concentration, the second term becomes important, and the rate law of the reaction can be modeled by the second order equation. This behavior has been reported, and the reaction was described to have mixed order [25]. The similar dependence relationship of k_{obs} on VA in the absence and presence of post-CMC concentrations of the surfactants proves the similar reaction mechanism in the absence and presence of micellar media.

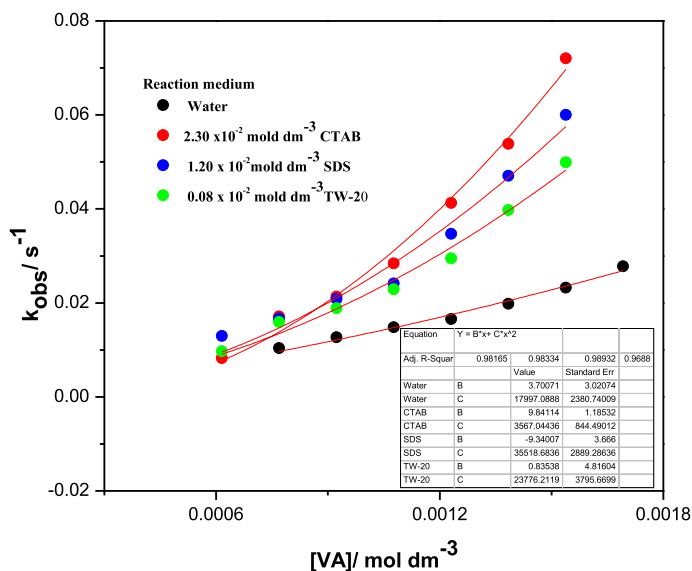


Fig. 3 k_{obs} vs. concentration of VA, in the absence and presence of surfactants; [colloidal MnO_2] $=1.54 \times 10^{-5}$ mol dm^{-3} , $[\text{H}_2\text{SO}_4]=1.20 \times 10^{-5}$ mol dm^{-3} , $[\text{Na}_2\text{SO}_4]=1.56 \times 10^{-2}$ mol dm^{-3} , at 298 K. The lines show the fitted experimental data to Eq. 3. The inset shows the regression parameters, $B = k$ and $C = \bar{k}$

Reaction order with hydrogen ion

The relation between k_{obs} and the concentration of hydrogen ions is shown in Fig. 4. The concentration of hydrogen ion was considered as twofold the concentration of added sulfuric acid. The plot is not linear, but the inset of Fig. 4 shows that the relation between the reciprocals of k_{obs} and $[\text{H}^+]$ is linear with a positive intercept at the vertical axis. This behavior is characteristic of the Michaelis–Menten kinetic model, which assumes that the order depends on the concentration of the reactant and ranges from 1 at very low concentration and 0 at sufficiently high concentration. The behavior also indicates that the role of hydrogen ion is catalytic. The reaction could proceed in the absence of the acid but at a slow rate. However, the rate was sensitive to hydrogen ions, and the addition of low concentrations of sulfuric acid resulted in a significant enhancement in the rate. The sensitivity became very low at higher acid concentrations, and k_{obs} reached saturation level. Therefore, the subsequent experiments were performed in a concentration of $1.20 \times 10^{-5} \text{ mol dm}^{-3}$ to keep the reaction kinetics trackable spectrophotometrically.

Salt effect

Several experimental runs were performed with varying the concentration of sodium sulfate and keeping other conditions fixed. No significant change in the value of k_{obs} was observed in response to the change in the salt concentration. This result

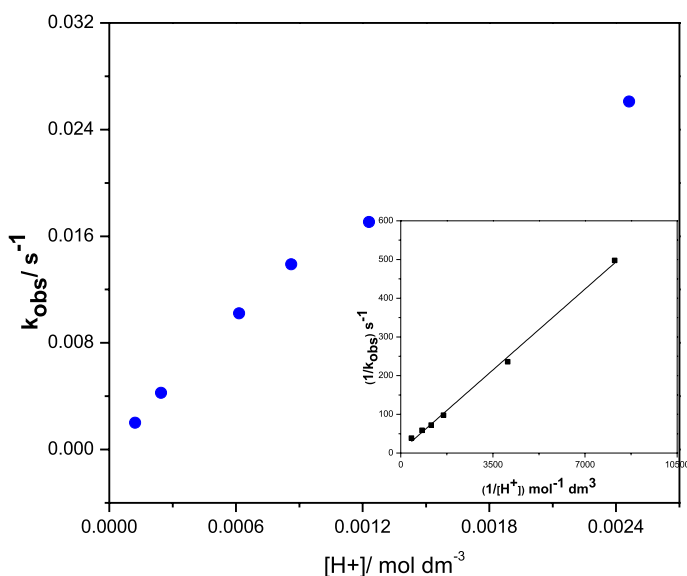


Fig. 4 k_{obs} vs. concentration of $[\text{H}^+]$; $[\text{VA}] = 7.70 \times 10^{-4} \text{ mol dm}^{-3}$, $[\text{colloidal MnO}_2] = 1.54 \times 10^{-5} \text{ mol dm}^{-3}$, $[\text{Na}_2\text{SO}_4] = 1.56 \times 10^{-2} \text{ mol dm}^{-3}$, at 298 K. The inset shows the fit of the plot between the reciprocals of k_{obs} and $[\text{H}^+]$ to a straight line

indicates that no effect of the ionic strength in the reaction rate. Consequently, the transition state of the slowest determining step is assumed to be a combination of either two neutral reactants or one of them is neutral and the other is charged [25].

Critical micelle concentration measurements

The critical micelle concentrations of pure SDS and CTAB and their mixed systems with TW-20 were measured by the conductivity method at 298 K. The obtained CMCs of SDS and CTAB were 8.05 mM and 1.97 mM, respectively. The first is in good agreement with the reported value, while that of CTAB is about double the literature reported [26]. The CMC of TW-20 was measured spectrophotometrically using methylene blue dye with λ_{\max} of 660 nm. The obtained value is 0.05 mM, which is very close to the reported value using the same technique [27].

Fig. 5 shows the conductivity vs. total concentration curves of some compositions of SDS-TW-20 mixed systems. Each curve shows two break points at lower and higher total surfactant concentrations. The two breaks correspond to the formation of two types of mixed micelles. Other authors have already confirmed the formation of two kinds of mixed micelles in SDS-TW-20 using both conductivity and surface tension methods [28]. The two CMCs are indicated by CMC_L and CMC_H and are presented in Table 1. The two CMCs descend to lower surfactant concentration with increasing the mole fraction of TW-20.

Fig. 6 shows the conductivity versus surfactant concentration curves of some compositions of CTAB-TW-20 mixed systems. Three breaks are observed at low,

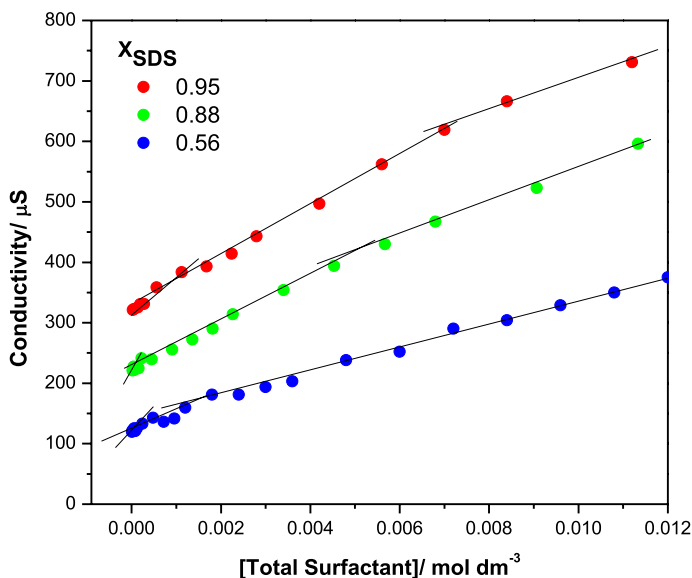
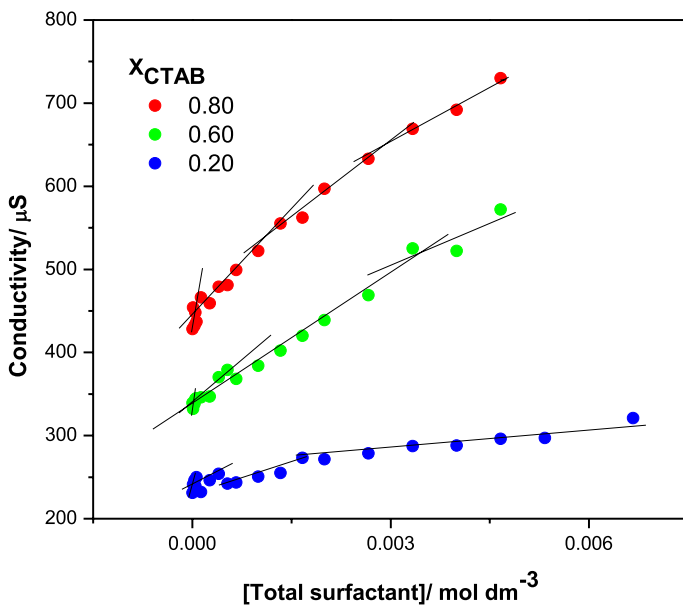


Fig. 5 Conductivity vs. total surfactant concentration of some compositions of CTAB-TW-20 mixed system at 298 K

Table 1 Measured CMCs, calculated CMCs, micellar mole fractions at ideal and non-ideal conditions, and interaction parameters of the mixed surfactant systems SDS-TW-20 and CTAB-TW-20

α (SDS)	$CMC_L/10^{-4} \text{ mol dm}^{-3}$	$CMC_H/10^{-4} \text{ mol dm}^{-3}$	$CMC^{id}/10^{-4} \text{ mol dm}^{-3}$	x^{id}	x_1	β
SDS-TW-20 mixed systems						
1.00	80.00	–	–	–	–	–
0.95	5.60	74.00	8.10	0.096	0.256	– 2.430
0.88	2.60	65.00	3.60	0.040	0.262	– 4.063
0.56	0.63	20.00	1.00	0.006	0.237	– 6.856
0.36	0.58	5.20	0.70	0.003	0.242	– 8.255
α (CTAB)	$CMC_L/10^{-4} \text{ mol dm}^{-3}$	$CMC_H/10^{-4} \text{ mol dm}^{-3}$	$CMC^{id}/10^{-4} \text{ mol dm}^{-3}$	x^{id}	x_1	β
CTAB-TW-20 mixed systems						
1.00	20.00	–	–	–	–	–
0.80	1.34	11.00	2.06	0.083	0.233	– 2.492
0.6	0.55	5.400	1.10	0.033	0.209	– 4.067
0.2	0.47	4.200	0.56	0.006	0.262	– 7.377

**Fig. 6** Conductivity vs. total surfactant concentration of some compositions of CTAB-TW-20 mixed system at 298 K

intermediate, and high surfactant concentrations. The first break occurs at a concentration close to that of TW-20, which can be attributed to the formation of TW-20 enriched mixed micelles and is accompanied by a large slope difference. The change in the slopes in the second and third breaks is relatively small. Consequently, micellar structure modification is the most probable reason for the second and third breaks. It was suggested that micelles might adopt different structures at higher post-micellar concentrations to overcome the increased electrostatic repulsions between charged micellar surfaces [29]. The concentration corresponding to the three breaks decreased with increasing the mole fraction of TW-20 in the mixture.

The ideal CMC for each mixed system has been calculated using the following equation [30]:

$$CMC^{id} = \alpha CMC_2 + (1 - \alpha) CMC_1 \quad (4)$$

Here CMC_1 and CMC_2 are the critical micelle concentrations of the more and less hydrophilic components, respectively, and α is the mole fraction of more hydrophilic surfactant in the mixture. The mole fraction in the mixed micelle in the ideal mixture, x^{id} , is then calculated from the equation:

$$x^{id} = \frac{CMC_2 \alpha}{CMC_2 \alpha + CMC_1 (1 - \alpha)} \quad (5)$$

The obtained CMC^{id} and x^{id} values at different mole fractions of SDS are given in Table 1. In comparison, it is found that the experimental CMC is lower than predicted by considering an ideal solution. This result indicates negative deviation from ideality which results from the interaction between the head groups of the two types of surfactants. Therefore, we considered Rubingh's regular solution theory [31] to calculate the non-ideal micellar mole fraction (x_1) and interaction parameter (β) in the real mixtures using the following two equations:

$$\frac{x_1^2 \ln(CMC^{ex} \alpha / CMC_1 x_1)}{(1 - x_1) \ln\left(\frac{CMC^{ex}(1-\alpha)}{CMC_2(1-x_1)}\right)} = 1 \quad (6)$$

$$\beta = \frac{\ln(CMC^{ex} \alpha / CMC_1 x_1)}{(1 - x_1)^2} \quad (7)$$

Here CMC^{ex} is the experimental CMC. The calculations were performed for the first CMC (CMC_L) measured by conductivity for the two types of mixed systems. Equation 6 has been solved by iteration to obtain the value of x_1 , which is then used to calculate β from Eq. 7. The calculated x_1 and β values of some compositions of CTAB-TW-20 and SDS-TW-20 mixed systems were added to Table 1.

The higher micellar mole fraction of SDS in the real mixture than in the ideal mixture indicates synergetic interaction between the two surfactants. This is also evidenced by the negative value of the interaction parameter. Moreover, the magnitude of the interaction parameter increases with increasing the mole fraction of

TW-20. TW-20 structure contains several oxyethylene groups, which play a significant role in the interaction with the sulfate head group of SDS. Hydrogen bonding might be the predominant interaction between the two surfactants. It is worth mentioning that the micellar mole fraction (x_1) changes less significantly with the change in the composition of the mixture. Besides, the results indicate that micelles are always TW-20 enriched in the whole composition range.

Similarly, as shown in Table 1, the experimental CMCs of CTAB-TW-20 mixed systems are lower than expected from ideal behavior. Again, the negative deviation is evidenced by the negative values of the interaction parameter. Interestingly, the interaction parameter increased with increasing TW-20 mol fraction, which is due to the higher number of functional groups across TW-20 structure. The expected predominant interaction between the head groups of CTAB and TW-20 is dipole–dipole interaction since the positively charged nitrogen atom in the ammonium head group cannot form hydrogen bonds. As a result, the interaction parameters in CTAB-TW-20 are smaller than those of similar compositions of SDS-TW-20.

Catalysis by single surfactants

Fig. 7 shows the variation of the ratio k_{obs}/k_w as a function of concentrations of the three surfactants TW-20, SDS, and CTAB. The addition of TW-20 in tiny concentration resulted in a sharp increase in the value of k_{obs} to about 1.3 times the value in pure water, followed by a rapid decrease, and finally attained a constant value with a further increase in surfactant concentration. The concentration that corresponds

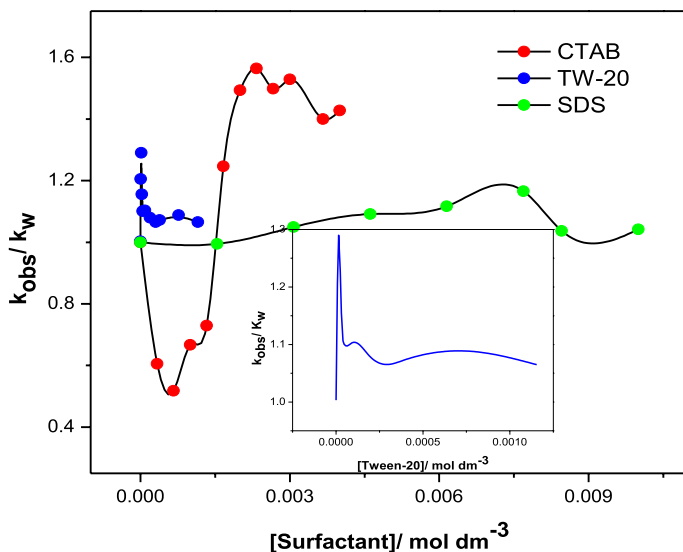


Fig. 7 k_{obs}/k_w vs. concentration of the three surfactants CTAB, SDS, AND TW-20; $[VA]=7.7 \times 10^{-4} \text{ mol dm}^{-3}$, $[\text{colloidal MnO}_2]=1.54 \times 10^{-5} \text{ mol dm}^{-3}$, $[\text{Na}_2\text{SO}_4]=1.56 \times 10^{-2} \text{ mol dm}^{-3}$, $[\text{H}_2\text{SO}_4]=1.20 \times 10^{-5} \text{ mol dm}^{-3}$, at 298 K. The inset is a magnification of TW-20 curve

to the hub in the curve ($0.038 \times 10^{-5} \text{ mol dm}^{-3}$) was in good close to the measured CMC of TW-20. This abrupt rise in the k_{obs} at CMC concentration is due to the enhanced solubility of the substrate in the micellar pseudo-phase. The solubilization process concentrates the substrate in a tiny volume in the micellar core. Increasing the concentration beyond CMC, however, caused micellar dilution, and again the k_{obs} diminished to a lower and almost constant value, which remains above that in pure water. Hence the observed limited catalytic behavior is expected to be due to the enhancement of solubility of the substrate.

As shown in Fig. 7, the catalytic profile of SDS shows similar behaviors except that the hub in k_{obs} value occurred at a higher concentration ($0.0065 \text{ mol dm}^{-3}$). This value is slightly lower than the CMC of SDS may be due to the reaction mixture's ionic strength. Besides, the width of the hub is more broadened than that observed with TW-20. The difference in the hub width between the two surfactants may be related to the kinetics and thermodynamics of micellization in the two cases. For example, the relaxation time for the formation-disintegration of micelle was slower with non-ionic surfactants than ionic surfactants [32].

The catalytic profile of CTAB showed a different pattern. First, an inhibition is observed at sufficiently low concentration followed by a major and sudden rise in the k_{obs} at a concentration of ($0.00147 \text{ mol dm}^{-3}$), which is also slightly lower than the measured CMC of CTAB. After CMC, the curve starts to descend slowly with a further increase in surfactant concentration. The inhibition at pre-micellar concentration can be attributed to a rise in the medium viscosity in the presence of CTAB monomers. The maximum k_{obs} in the presence of CTAB was about 1.6-fold that in pure water. In comparing with TW-20 and SDS, it is found that CTAB is more efficient in catalyzing the titled reaction.

Based on the previous discussion, the hub in each surfactant's catalytic profile occurred at a concentration comparable to the CMC obtained from the conductivity method. The difference in the two concentrations results from the ionic strength of the reaction mixture since the conductivity measurements were carried out for the surfactants in water. Therefore, micellar catalytic measurements of single surfactants can produce CMCs with acceptable accuracy.

Catalysis by mixed SDS-TW-20 and CTAB-TW-20 systems

The variations of k_{obs} values with a total surfactant concentration of some compositions of the SDS-TW-20 mixed system are sketched in Fig. 8. The three curves show a first sudden rise at concentrations very close to the CMC of TW-20. At higher concentration segments, a second gradual increase is observed close to the CMC of SDS. The concentration corresponding to the first rise shows slight variation with the composition of the mixture, while that of the second decreased rapidly with decreasing SDS content. Each curve in Fig. 8 consists of two parts, the first part (at low concentration) resembles the curve of pure TW-20, while the second segment is very similar to SDS (see Fig. 7). It appears that the interaction between the two surfactants does not significantly affect the behavior of the two surfactants to act as a single system. Therefore, as evidenced by the nature of the

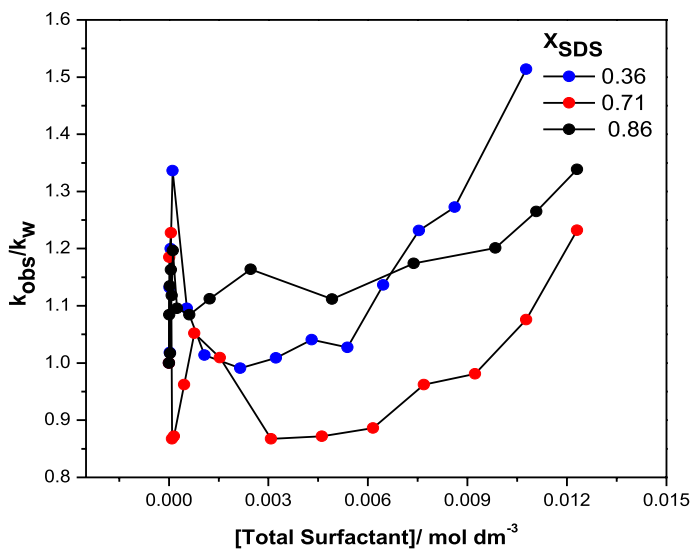


Fig. 8 k_{obs}/k_w vs. concentration of three surfactants compositions of mixed system CTAB, SDS-TW-20; $[\text{VA}] = 7.70 \times 10^{-4} \text{ mol dm}^{-3}$, $[\text{colloidal MnO}_2] = 1.54 \times 10^{-5} \text{ mol dm}^{-3}$, $[\text{Na}_2\text{SO}_4] = 1.56 \times 10^{-2} \text{ mol dm}^{-3}$, $[\text{H}_2\text{SO}_4] = 1.20 \times 10^{-5} \text{ mol dm}^{-3}$, at 298 K

curves in Fig. 8, we assume that TW-20 enriched micelles are formed at a low concentration range. However, as the surfactant concentration approaches CMC of SDS, enriched SDS mixed micelles become predominant. The formation of mixed micelles is evidenced by the variations in the concentrations at which the k_{obs} rise occur in either segment with the composition of the mixed system.

Fig. 9 shows the variation of k_{obs} as a function of the total concentration of the mixed system CTAB-TW-20. The composition with a low CTAB mole fraction (0.08) shows inhibition of reaction rate at very low surfactant concentration, then a sudden catalytic action is observed. The early inhibition with this particular composition could be due to the increased viscosity of the reaction medium, while the latter catalysis is attributed to the initiation of micelles formation. The other three compositions did not show the earlier inhibition, and only sudden k_{obs} hub at a specific range of surfactant concentrations are observed. In general, the onset of catalytic activity occurs at concentrations close to the CMC of pure TW-20. There is no apparent variation in the onset concentration with changing the composition of the mixture. The catalytic profiles do not show other characteristics that correspond to the change in the micellar structure that was observed in the conductivity curves. It turns out that the kinetic measurements are insensitive to the change in the micellar morphology. The maximum rate constant achieved with CTAB-TW-20 mixed system exceeds threefold the value in water. The change in the composition does not result in a significant change in the maximum rate obtained. The maximum k_{obs} in the presence of the CTAB-TW-20 mixed system exceeds those obtained by single surfactants, which suggests a

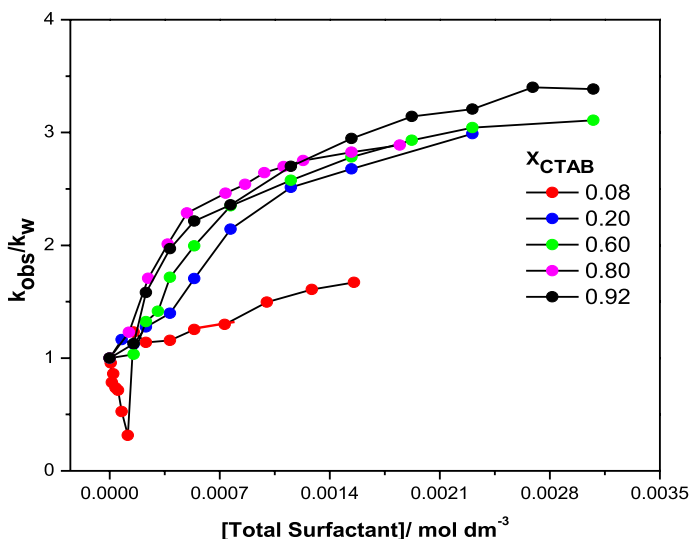


Fig. 9 k_{obs}/k_w vs. total surfactant concentration of three compositions of mixed system CTAB-TW-20; $[\text{VA}] = 7.70 \times 10^{-4} \text{ mol dm}^{-3}$, $[\text{colloidal MnO}_2] = 1.54 \times 10^{-5} \text{ mol dm}^{-3}$, $[\text{Na}_2\text{SO}_4] = 1.56 \times 10^{-2} \text{ mol dm}^{-3}$, $[\text{H}_2\text{SO}_4] = 1.20 \times 10^{-5} \text{ mol dm}^{-3}$, at 298 K

synergetic catalytic behavior of the system on the titled reaction. Besides, there is also a reduction in the concentration at which catalytic action is shown up.

In comparing the obtained micellar properties of both types of mixed systems studied by conductivity and micellar catalysis methods, it is concluded that there is an agreement in the estimation of the concentrations at which mixed micelles form (CMCs). Nevertheless, the other breaks in the conductivity curves that may correspond to the variation in the micellar structure were not reflected in the catalytic profiles. Therefore, the micellar catalysis measurements profile can be used to detect micelles formation. Still, they are insensitive to the variations in the micellar morphology, which are generally observed at post-micellar concentration using conductivity or surface tension techniques.

Application of pseudo-phase model to the micellar catalysis

To get more insights about the micellar catalysis on the reaction, the Pseudo-phase model developed by Menger and Portnoy was applied to the catalytic of this work [33]. The applicable equation of the model can be written as in the following form:

$$\frac{1}{k_w - k_{\text{obs}}} = \frac{1}{k_w - k_m} + \left(\frac{1}{k_w - k_m} \times \frac{1}{KC} \right) \quad (8)$$

Here, k_w and k_m is the observed rate constant in the absence and presence of surfactant, C the concentration of the micelles, can be obtained by subtracting the CMC from the added surfactant concentration, and K is the binding constant of the

Table 2 The micellar rate constant k_m , binding constant K , and the ratio k_m/k_w , which result from the application of the pseudo-phase model to the micellar catalysis

Surfactant	$10^{-2} \text{ km/s}^{-1}$	$\text{K/mol}^{-1}\text{dm}^3$	k_m/k_w	r^2
CTAB	1.52	395.38	1.90	0.962
SDS	0.91	7930.71	1.14	0.987
TW-20	0.88	58,980.38	1.10	0.973
0.8CTAB-0.2TW-20	2.45	4556.73	3.07	0.993
0.6CTAB-0.4TW-20	4.73	424.29	5.91	0.957
0.86SDS-0.14TW-20	0.87	14,799.39	1.09	0.955
0.36SDS-0.64RW-20	0.94	157.30	1.18	0.950

The regression coefficients of the linear fitting to Eq. 8 are also given

substrate to the micelle. The model was applied satisfactorily to the data and produced fitted straight lines with an acceptable regression coefficient (Table 2). The rate constants and binding constants calculated from the intercepts and slopes of the straight lines are also given in Table 2. The k_m of CTAB is about twice k_w , while those of SDS and TW-20 are almost comparable to it. Hence, CTAB is more efficient in the catalysis of the titled reaction.

The values of the binding constant K show opposite order; the values are significantly high with SDS and TW-20 and moderate with CTAB. The higher the binding constant, the stronger is the binding of the substrate to the micellar structure. It appears that the oxygen atom-containing head groups can bind the substrate stronger by the formation of hydrogen bonds. This possibility is not facilitated with CTAB since quarterly coordinated nitrogen atoms cannot form hydrogen bonds. In general, the binding of the substrate to the micelle is necessary for catalytic action. However, excessive binding may retard the reaction in the micellar pseudo-phase. It may indicate strong binding of the product to the micellar structure and retard its release to provide more catalytic sites to other substrate molecules. The pseudo-phase model is based on the distribution and rapid exchange of the substrate between the bulk and micellar media.

The magnitude of the binding constant, in this case, maybe correlated to the shape of the catalytic profile. As seen in the catalytic profile of TW-20 in Fig. 7, k_{obs} drop rapidly from the maximum value, and the curve is very steeping. Martinek et al., in their model of micellar catalysis, pointed out this remark [34]. They correlated the shape of the catalytic profile to the substrate's distribution coefficient between the micellar and bulk phases, K_D , and the ratio k_m/k_w . The lower the distribution coefficient and the higher k_m/k_w indicates a more broadened peak and less steep drop after passing the maximum and vice versa. The binding constant of the substrate can be correlated to the distribution coefficient so that the higher the binding constant, the higher is the K_D . Based on this argument, the narrow and post maximum steeping curve in the profile of TW-20 may be attributed to the extremely higher K_D and relatively less k_m/k_w . A similar discussion can be adapted to the catalytic profiles of SDS and CTAB. The peaks in the catalytic profiles increasingly become more broadened with decreasing binding constants and increasing the k_m/k_w . The model was applied to some mixed CTAB-TW-20 and SDS-TW-20 systems, and

the calculated catalytic parameters were also added to Table 2. The mixed system 0.6CTAB-0.4TW-20 exhibited the highest k_m/k_w , which is evidence of strong synergistic interaction.

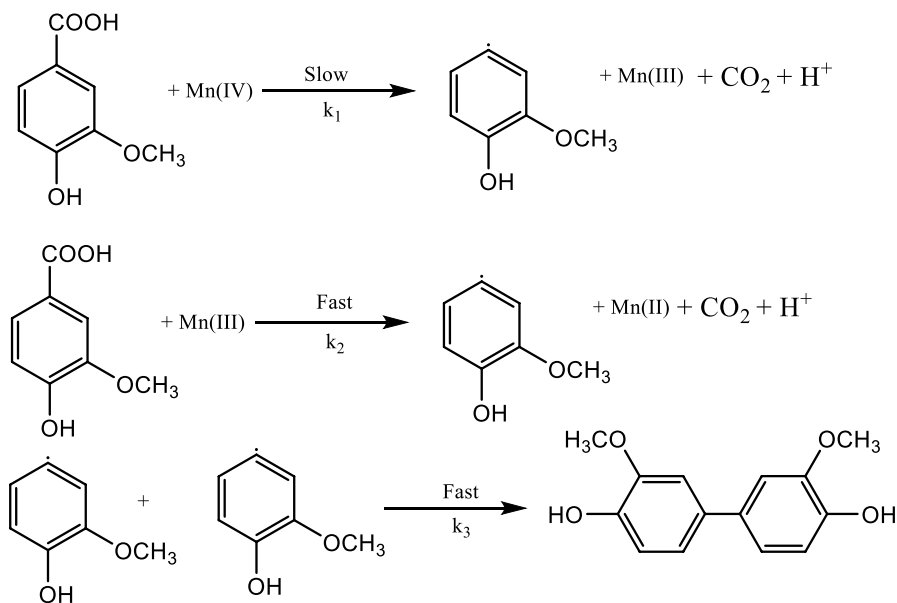
Mechanism

The reaction at a sufficiently low concentration of VA is expected to proceed via the mechanism depicted in Scheme 1. The conversion of VA to free radical is likely to proceed in two steps. In the first step, one molecule of VA is converted to a free radical, and Mn(IV) is reduced to Mn(III). The second molecule of VA reacts with Mn(III) in a second step to form another free radical. The combination of the two free radicals gives the final product (HULIS). Because Mn(III) compounds are less stable than Mn(IV) [35], the second step is expected to be much faster than the first. Therefore, the first step could be considered to be the determining step. The rate constant at low VA concentration that can be devised from this mechanism:

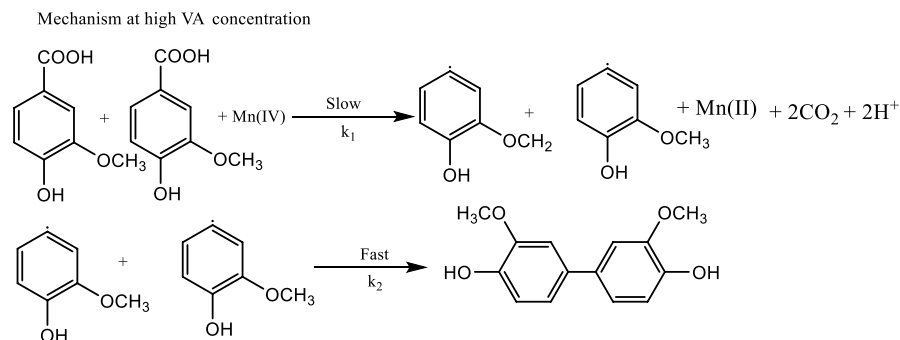
$$R = k_1[VA][Mn(IV)] \quad (9)$$

At a higher concentration, the mechanism changes to that depicted in Scheme 2. Therein, two molecules are converted to free radicals simultaneously, and Mn(IV) is reduced to the final stable Mn(II). Then, the two free radicals combine in a second

Mechanism at low VA concentration



Scheme 1 Mechanism of oxidation of VA by colloidal MnO₂ at sufficiently lower [VA]



Scheme 2 Mechanism of oxidation of VA by colloidal MnO₂ at sufficiently high [VA]

step to form the HULIS. The first step is expected to be the slowest determining step, and the overall rate can be written as:

$$R = k_1 [VA]^2 [Mn(IV)] \quad (10)$$

Conclusion

The kinetics of oxidation of VA by colloidal MnO₂ was studied at micellar media of the surfactants CTAB, SDS, and TW-20 and mixed systems of CTAB-TW-20 and SDS-TW-20. The reaction was found to be first order with respect to colloidal MnO₂, mixed order with respect to VA, and fractional order with respect to H⁺. The presence of post-micellar concentrations of the three surfactant and mixed surfactant systems enhanced the reaction rate. The catalytic profiles were correlated with micellar properties of the three surfactants and mixed systems. It is concluded that micellar catalytic measurements could provide information about the formation of micelles and mixed micelles but incapable of exploring the variations in the micellar structures with the variations in the systems' composition. The pseudo phase model was used to separate the reaction rates in the presence and absence of micellar medium and to correlate the shape of the catalytic profiles to the molecular interaction between the reactants and micelles.

Acknowledgements Mohammed Hassan is grateful to IIE, New York, for granting him an SRF fellowship.

Declarations

Conflict of interest No conflicts of interest of any type are related to this work.

References

1. Massarweh O, Abushaikh AS (2020) The use of surfactants in enhanced oil recovery: a review of recent advances. *Energy Rep.* <https://doi.org/10.1016/j.egy.2020.11.009>
2. Tharwat FT (2005) *Applied surfactants: principles and applications*. Wiley, Weinheim
3. Dwars T, Paetzold E, Oehme G (2005) Reactions in micellar systems. *Angew Chem Int Ed.* <https://doi.org/10.1002/anie.200501365>
4. Vafakish B, Wilson LD (2021) A review on recent progress of glycan-based surfactant micelles as nanoreactor systems for chemical synthesis applications. *Polysaccharides.* <https://doi.org/10.3390/polysaccharides2010012>
5. Samant BS, Bhagwat SS (2012) Selectivity enhancement of aromatic halogenation reactions at the micellar interface: effect of highly ionic media. *Monatsh Chem.* <https://doi.org/10.1007/s00706-011-0677-1>
6. Holland P, Rubingh D (1992) Mixed surfactant systems - an overview. *ACS Symp Ser.* <https://doi.org/10.1021/bk-1992-0501.ch001>
7. Kanoje B, Padshala S, Parikh J, Sahoo SK, Kuperkar K, Bahadur P (2017) Synergism and aggregation behaviour in an aqueous binary mixture of cationic-zwitterionic surfactants: physico-chemical characterization with molecular simulation approach. *Phys Chem Chem Phys.* <https://doi.org/10.1039/C7CP05917E>
8. Umoruddin NS, Rosdi MH, Ariffin A (2019) Mixed surfactant enabled EVA emulsion for PPD applications. *J Dispers Sci Technol.* <https://doi.org/10.1080/01932691.2018.1469413>
9. Cui X, Jiang Y, Yang C, Lu X, Chen H, Mao S, Liu M, Yuan H, Luo P, Du Y (2010) Mechanism of the mixed surfactant micelle formation. *J Phys Chem B.* <https://doi.org/10.1021/jp101032z>
10. Sachin KM, Karpe SA, Singh M, Bhattarai A (2019) Self-assembly of sodium dodecylsulfate and dodecyltrimethylammonium bromide mixed surfactants with dyes in aqueous mixtures. *R Soc Open Sci.* <https://doi.org/10.1098/rsos.181979>
11. Hassan M, Al-Hazmi SM, Alhagri IA, Alhakimi AN, Dahadha A, Al-Dhoun M, Batineh Y (2021) Micellar catalysis of chemical reactions by mixed surfactant systems and gemini surfactants. *Asian J Chem* <https://doi.org/10.14233/ajchem.2021.23187>
12. Almoazen H, Simonelli AP (2008) Determining the critical micelle concentration in O/W emulsion using the rate constant of hydrolysis for benzyl acetate. *J Dispers Sci Technol.* <https://doi.org/10.1080/01932690701808445>
13. Janet RJ, Jeevi RR, Subramaniam P (2019) Synergistic interaction of mixed micelles evidenced by kinetic investigation. *Int J Res Anal Rev* 6(1):492–500
14. Mondal MH, Ali MA, Pal A, Saha B (2019) A review on micellar catalyzed oxidation reactions of organic functional groups in aqueous medium using various transition metals. *Tenside Surfactants Deterg.* <https://doi.org/10.3139/113.110654>
15. Altaf M, Jaganyi D (2013) Oxidation of methionine by colloidal MnO₂ in aqueous and micellar media: a kinetic study. *J Dispers Sci Technol.* <https://doi.org/10.1080/01932691.2012.751029>
16. Akram M, Altaf M, Kabir-ud-Din A-T (2012) Kinetics and mechanism of the reduction of colloidal MnO₂ by glycyl-leucine in the absence and presence of surfactants. *J Saudi Chem.* <https://doi.org/10.1016/j.jscs.2010.12.009>
17. Akram M, Altaf M, Kabir-ud-Din (2012) Oxidative degradation of dipeptide (glycyl-glycine) by water-soluble colloidal manganese dioxide in the aqueous and micellar media. *Colloids Surf B.* <https://doi.org/10.1016/j.colsurfb.2010.08.044>
18. Sun B, Xiao Z, Dong H, Ma S, Wei G, Cao T, Guan X (2019) Bisulfite triggers fast oxidation of organic pollutants by colloidal MnO₂. *J Hazard Mater.* <https://doi.org/10.1016/j.jhazmat.2018.10.002>
19. Islam MA, Rahman MM (2019) Soluble colloidal manganese dioxide: formation, identification and prospects of application. *Colloid J.* <https://doi.org/10.1134/S1061933X13050049>
20. Pietta PG, Simonetti P, Gardana C, Brusamolino A, Morazzoni P, Bombardelli E (1998) Catechin metabolites after intake of green tea infusions. *BioFactors.* <https://doi.org/10.1002/biof.5520080119>
21. Perez-Benito JF, Arias C (1992) A kinetic study of the reaction between soluble (colloidal) manganese dioxide and formic acid. *J Colloid Interface Sci.* [https://doi.org/10.1016/0021-9797\(92\)90394-2](https://doi.org/10.1016/0021-9797(92)90394-2)

22. Tang S, Li F, Tsona NT, Lu C, Wang X, Du L (2020) Aqueous-phase photooxidation of vanillic acid: a potential source of humic-like substances (HULIS). ACS Earth Space Chem. <https://doi.org/10.1021/acsearthspacechem.0c00070>
23. Ghosh DC (2018) Effect of microheterogeneous environments of CTAB, Triton X-100, and Tween 20 on the oxidative degradation of D -fructose by nanoparticles of MnO₂. Int J Chem Kinet. <https://doi.org/10.1002/kin.21239>
24. Perrin CL (2017) Linear or nonlinear least-squares analysis of kinetic data? J Chem Educ. <https://doi.org/10.1021/acs.jchemed.6b00629>
25. Espenson JH (1981) Chemical kinetics and reactions mechanisms. McGraw-Hill, New York
26. Tiwari S, Mall C, Solanki PP (2019) CMC studies of CTAB, SLS & tween 80 by spectral and conductivity methodology to explore its potential in photogalvanic cell. Surf Interfaces. <https://doi.org/10.1016/j.surfin.2019.100427>
27. Patist A, Bhagwat SS, Penfield KW, Aikens P, Shah DO (2000) On the measurement of critical micelle concentrations of pure and technical-grade nonionic surfactants. J Surfactants Deterg. <https://doi.org/10.1007/s11743-000-0113-4>
28. Rodri A, Graciani M, Moya L (2004) Conductometric, surface tension, and kinetic studies in mixed SDS - Tween 20 and SDS - SB3-12 Micellar solutions. Langmuir. <https://doi.org/10.1021/la048247n>
29. Rafique AS, Khodaparast S, Poulos AS, Sharratt WN, Robles EJ, Cabral JT (2020) Micellar structure and transformations in sodium alkylbenzenesulfonate (NaLAS) aqueous solutions: effects of concentration, temperature, and salt. Soft Matter. <https://doi.org/10.1039/D0SM00982B>
30. Kronberg B, Holmberg K, Lindman B (2014) Surface chemistry of surfactants and polymers. Wiley, New York
31. Rubingh DN (1979) Mixed Micelle solutions. In: Mittal KL (eds) Solution chemistry of surfactants. Springer, Boston
32. Patist A, Oh SG, Leung R, Shah DO (2001) Kinetics of micellization : its significance to technological processes. Colloids Surf A. [https://doi.org/10.1016/S0927-7757\(00\)00610-5](https://doi.org/10.1016/S0927-7757(00)00610-5)
33. Acharjee A, Rakshit A, Chowdhury S, Saha B (2020) Micelle catalyzed conversion of “on water” reactions into “in water” one. J Mol Liq 321:114897. <https://doi.org/10.1016/j.molliq.2020.114897>
34. Martinek K, Yatsimirski AK, Levashov AV, Berezin IV (1977) The kinetic theory and the mechanisms of micellar effects on chemical reactions. Micellization Solubilization Microemulsions. https://doi.org/10.1007/978-1-4613-4157-4_14
35. Lee RH (2015) Investigating the stability of aqueous Mn(III) in the presence of humic substances and measuring manganese speciation with alpha, beta, gamma, delta-tetrakis (4-carboxyphenyl)porphine. Master Thesis. <http://hdl.handle.net/11124/20115>

Publisher's Note Springer Nature remains neutral with regard to jurisdictional claims in published maps and institutional affiliations.